# Study on the Influence of an UGV Suspension System on Camera Motion of the Teleoperation System

Arkadiusz Rubiec, Mirosław Przybysz, Marian J. Łopatka, Łukasz Rykała, Piotr Krogul, Karol Cieślik, Rafał Typiak
Military University of Technology, Faculty of Mechanical Engineering, ul. gen. Sylwestra Kaliskiego 2, 00-908 Warsaw, Poland

Abstract: In the following article, the results of a study on the impact of the suspension system used in Unmanned Ground Vehicles (UGVs) on the kinematic excitation of cameras in teleoperation systems are presented. As indicated by preliminary reconnaissance studies, these excitations significantly affect the operator's ability to perceive the environment and recognize images while driving. Currently, there is a lack of publications and guidelines in the literature regarding the design of UGV suspensions and their evaluation in terms of improving operator perception in teleoperation systems. The studies were conducted in a simulated environment using multibody systems, where various suspension structure variants were developed. The tests were carried out on the ISO 5008 rough test track. The evaluation of the tested suspension structures was carried out using a proprietary method, enabling parametric analysis and the selection of favorable solutions for improving image recognition by the UGV operator. Future research can focus on adjustment of the UGV suspension characteristics which could have significant influence on situational awareness and the operator's ability to act effectively, especially during dynamic missions.

**Keywords:** suspension system, teleoperation system, UGV, situational awareness, multibody model

## 1. Introduction

Human activity in areas that require performing monotonous, complex, and time-consuming tasks [27], especially where health and life can be at risk, has led to significant interest in the possibility of robotizing such operations and developing unmanned technologies [21]. Advanced systems increase the autonomy levels of the mentioned technologies [12, 23], yet they are defined differently for mobile robots (rescue, military), vehicles, or industrial robots [10]. Thanks to this approach, there is a reduction in human involvement and participation in task execution, which leads to a minimization of their psychophysical strain. Ultimately, as a result, tasks can be conducted with greater efficiency and repeatability.

In recent times, there has been a significant technological leap in increasing achieved levels of autonomy, particularly in the case of cars and industrial robots [38, 24, 30]. Both move and perform tasks in a known and structured environment [40, 7]. Cars, for instance, travel on a known road where familiar and defined objects appear (other vehicles, horizontal and vertical road signs, etc.), and a GNSS signal is typically available, which, supported by RTK corrections, ensures high location accuracy [33]. On the other hand, industrial robots usually perform tasks in industrial halls where every object in their working field can be defined.

Nevertheless, there are still areas where increasing level of autonomy is decidedly more challenging, and often an operator must take control over task execution, possibly remotely controlling the robot, for instance, in a teleoperation system [36]. This can occur, especially when robots are designated to perform tasks in tough, unfavorable terrain conditions, in an unknown, heterogeneous, and dynamically changing environment that is difficult to define. Examples include unmanned ground vehicles and mobile robots used in rescue operations after natural disasters or during military actions [4, 13]. They move over numerous irregularities and overcome significant terrain obstacles, which exert forces through the drivetrain and suspension onto the robot's structure, and subsequently onto the teleoperation system's cameras, thereby complicating the operator's task and reducing their situational and operational awareness [8, 14, 11]. The challenge in this case is to shape the force transfer path to the teleoperation system's cameras in a way that minimizes their adverse effects.

One possible direction is to avoid a rigid connection of the cameras to the robot's structure and to utilize vibration isolation or actively controlled platforms (gimbals) [37, 31]. However, conducted analyses [25, 32] showed that this approach might be ineffective. In crisis situations, the image from the teleoperation system is the only signal based on which the operator builds awareness and makes decisions. The situation is different for

**Autor korespondujący:**
Mirosław Przybysz, miroslaw.przybysz@wat.edu.pl

**Artykuł recenzowany**
nadesłany 24.10.2023 r., przyjęty do druku 22.04.2024 r.

manned machines and vehicles where operators/drivers directly perceive the movements and vibrations of the machine/vehicle, allowing them to, for example, reduce speed when there is a risk of rollover instability and tipping of the machine/vehicle. In the case of UGVs, if the camera is stabilized and has a different angular position than the robot's structure, and the operator does not feel excessive tilts, it might lead to the robot's overturning and failure to complete the task.

A potential solution to this problem could be the design of the UGV's suspension system (both in structure and characteristics) that minimizes the negative impact of kinematic excitation on the teleoperation system's cameras, caused by ground irregularities it traverses. In the literature, numerous research findings dedicated to the design of suspension systems for machines and vehicles can be found [41, 3, 35]. They primarily focus on three criteria:

— health and comfort [6, 17, 39, 42] in terms of vibration frequency and amplitude;
— safety [22, 29] concerning stability and motion steadiness.

Research is also carried out on autonomous UGVs in the context of defense technology advancement [34], UGVs suspension designs tailored for desert terrains [2], and minefields [15]. Studies also explore hydropneumatic solutions used for heavy UGVs [20], accompanied by various controllers based, among others, on adaptive [26], adaptive sliding [5], or fuzzy [1] control systems.

Mentioned papers concern the adaptation of suspension properties to defined functions and requirements set for manned vehicles and machines, aimed at reducing the negative impact of ground unevenness on the human and the body frame. Existing ISO 2631 guidelines [18], such as recommendations regarding vibration frequency and total acceleration acting on a human, serve as a basis for designing suspension systems focused on enhancing comfort and safety. In the studies [2, 20, 15, 28, 19], research was conducted on shaping the suspension properties of UGVs. However, they primarily addressed the impact of the suspension system on the platforms' ability to overcome terrain obstacles [15] or develop traction force [19]. What is missing, however, are research findings regarding the impact of the properties (structure and characteristics) of the UGVs' suspension system on building situational and actionable awareness and the efficiency of task execution using teleoperated platforms. In this case, the movement of teleoperation cameras and, consequently, what the operator sees on the monitor screens can be significant. This pertains to tasks of reconnaissance and identification of objects/threats in the immediate vicinity of the platforms. Current existing indicators to evaluation of suspension systems are proper to manned vehicles and there are not taking into consideration unmanned character of mobile robots. It can be fulfilled by proposed approach. Study proposes a method for evaluating the influence of the suspension properties of unmanned ground platforms controlled in a teleoperation system on the movement of their cameras, and consequently, the operator's ability to recognize and identify.

## 2. Preliminary research

To evaluate the influence of the movement of the teleoperation system's cameras on the operator's ability to recognize and identify images, preliminary identification tests were conducted. The trials were performed with the participation of 30 operators aged between 27 and 42, controlling UGVs using a teleoperation system while driving along a test track (Fig. 1). During the tests, the operators' task was to recognize (locate) and identify (read) markers (Fig. 2), placed on the left and right of the test track at locations unknown to the operators. The UGV, during the test, traveled in a straight line over uneven terrain, causing angular accelerations of the vehicle's body [9].

During the research, the UGV traveled on the experimental test track, which had terrain irregularities (Fig. 2) [9]. The irregularities height was 0.15 m, and they were alternately placed on the left and right sides of the track every 3 m. During the tests, the UGV traveled at average speeds $v_j$ ($j = 1, ..., 5$) of 0.5; 0.7; 1.3; 2.5, and 3.4 m/s. An IMU sensor was mounted on the platform to measure kinematic quantities: angle, angular velocity, and angular acceleration of the vehicle body relative to the axes: 1 – longitudinal, 2 – vertical, and 3 – transverse.


**Fig. 1. A view of the vehicle and control station used during the research**
Rys. 1. Widok pojazdu i stanowiska sterowania używanego podczas badania

Main technical parameters of the vision and measurement systems used during the research are provided in Table 1.

**Tab. 1. Parameters of the vision and measurement system**
Tab. 1. Parametry systemu wizyjnego i pomiarowego

| Name of parameters | Value of the parameter |
|---|---|
| Number and type of cameras | Three LC – 1/3 Sony 650TVL |
| Converter | 1/3" Sony CCD |
| Resolution | TVL 650 |
| Sensitivity | 0.1 lux |
| Transmission system | BMS dedicated |
| Frequency | 1400 MHz |
| Number of channels | 3 |
| Time delay | 120 ms |
| IMU | VECTORNAV VN-100<br>Pitch/Roll Accuracy: 0.5 deg<br>Accel In-Run Bias Stability < 0.04 mg |

In the studies, the markers consisted of letters or numbers. Between trials, their positions were changed or swapped to avoid memory-based identification attempts. The control station (Fig. 1) was located in a closed room away from the track, thus operators did not have direct visual contact with the driving area.

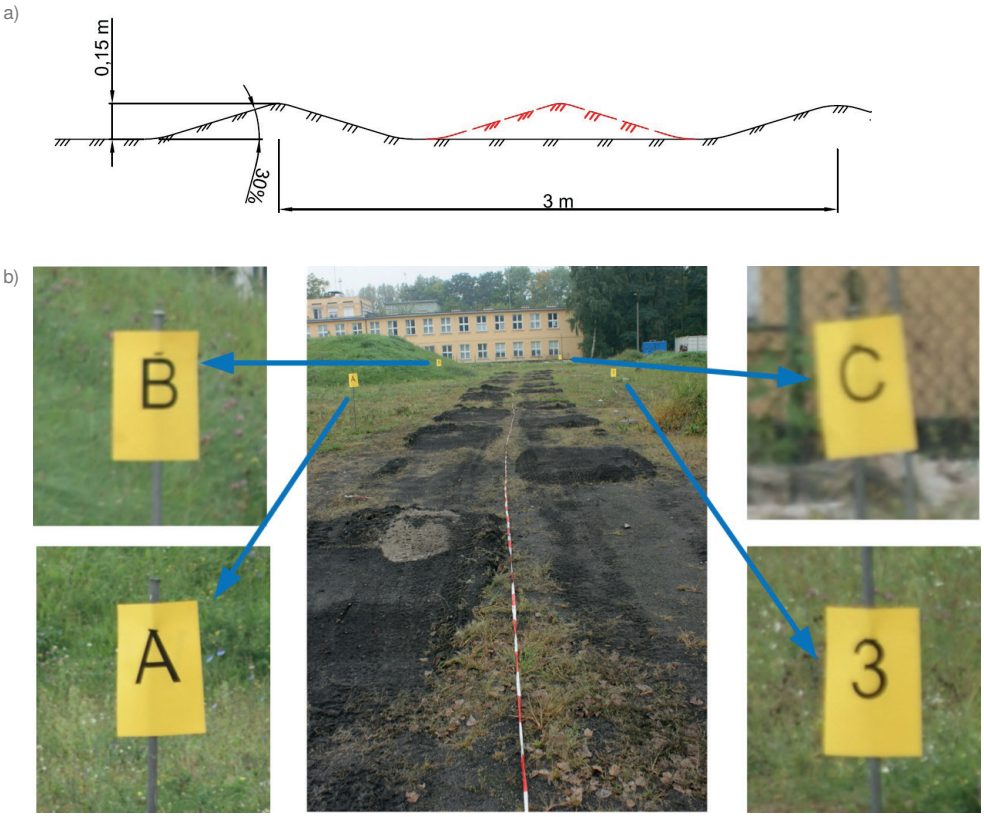


**Fig. 2. Test track: a) track profile; b) markers**
Rys. 2. Tor testowy: a) profil toru; b) znaczniki

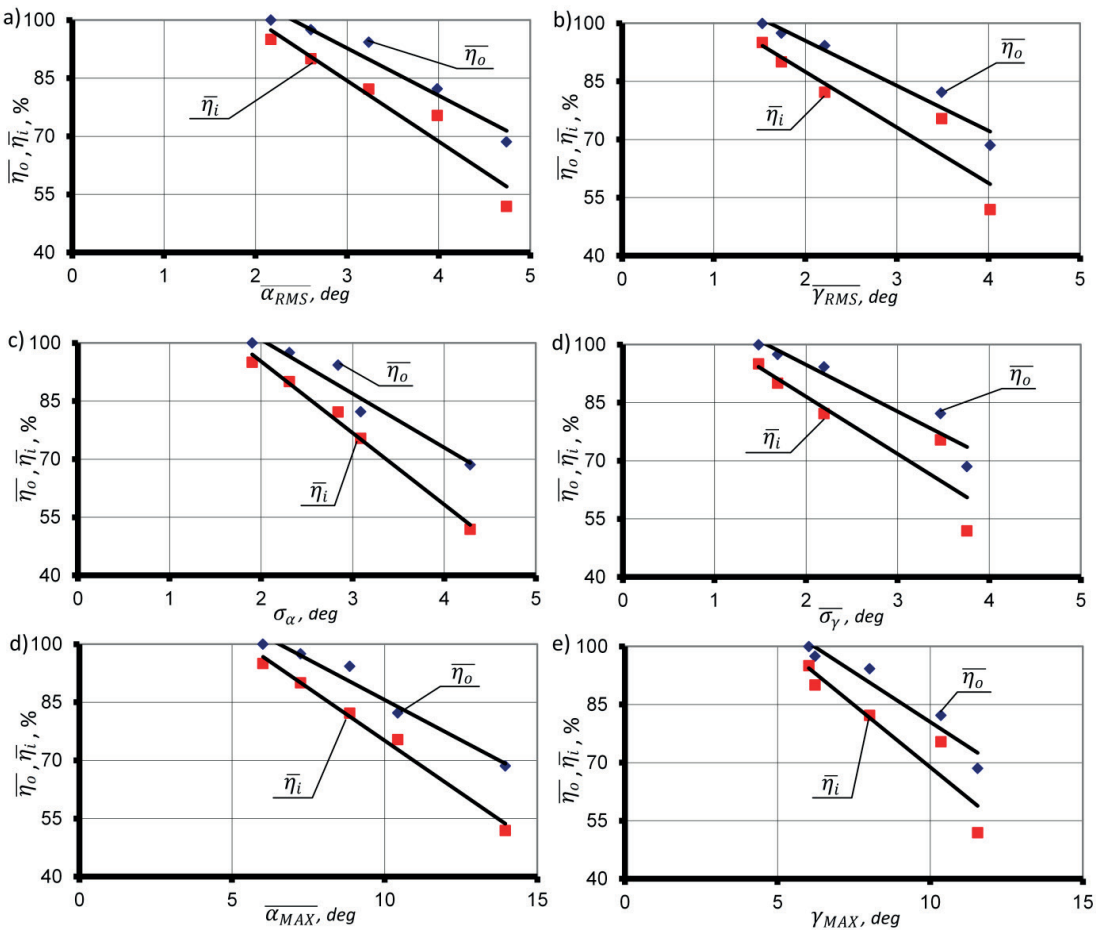


**Fig. 3. Changes in average efficiency indicators for locating markers $\overline{\eta_o}$ and identifying markers $\overline{\eta_i}$ function of average values: a) $\overline{\alpha_{RMS}}$; b) $\overline{\gamma_{RMS}}$; c) $\overline{\sigma_\alpha}$; d) $\overline{\sigma_\gamma}$; e) $\overline{\alpha_{MAX}}$; f) $\overline{\gamma_{MAX}}$**
**Rys. 3.** Zmiany wartości średnich wskaźników skuteczności odnajdowania znaczników $\overline{\eta_o}$ oraz identyfikacji znaczników $\overline{\eta_i}$ w funkcji średnich wartości: a) $\overline{\alpha_{RMS}}$; b) $\overline{\gamma_{RMS}}$; c) $\overline{\sigma_\alpha}$; d) $\overline{\sigma_\gamma}$; e) $\overline{\alpha_{MAX}}$; f) $\overline{\gamma_{MAX}}$

**Tab. 2. Classification of suspension system efficiency in remotely controlled wheeled UGVs based on marker identification**
Tab. 2. Klasyfikacja efektywności układu zawieszenia w sterowanych zdalnie kołowych UGV pod względem identyfikacji znaczników

| Suspension performance level | $\overline{\eta_o}$ [%] | $\overline{\eta_i}$ [%] | $\overline{\dot{\alpha}_{RMS}}$ [deg/s] | $\overline{\dot{\gamma}_{RMS}}$ [deg/s] | $\overline{\dot{\omega}_{RMS}}$ [deg/s] |
|---|---|---|---|---|---|
| Excellent | 100 | 100 | < 1.7 | < 1.4 | < 1.0 |
| Good | 100 | < 95–100) | (1.7–3.3 > | (1.4–2.6 > | (1.0–2.0 > |
| Acceptable | 100 | < 90–95) | (3.3–6.6 > | (2.6–4.5 > | (2.0–8.6 > |
| Unacceptable | < 100 | < 90 | > 6.6 | > 4.5 | > 8.6 |

To evaluate the efficiency of the task performed by the teleoperator, two indicators were used:

- a markers detection efficiency index $\eta_o$ calculated as the ratio of the number of markers found by the operator during a single drive $i_o$ to the total number of markers placed on the route $i_c$ during that drive, according to the equation:

$$\eta_o = \frac{i_o}{i_c} \cdot 100\ \% \tag{1}$$

- a markers identification efficiency index $h_i$ calculated as the ratio of the number of identified markers by the operator during a single drive $i_i$ to the number of markers found $i_o$ during that drive, according to the equation:

$$\eta_i = \frac{i_i}{i_o} \cdot 100\ \% \tag{2}$$

During each drive, the number of markers found, and the number of markers identified were noted. Cameras head motion were described by:
- average of angular displacement $RMS$ values of the camera head around the longitudinal axis $\overline{\alpha_{RMS}}$;
- average of angular displacement $RMS$ values of the camera head around the transverse axis $\overline{\gamma_{RMS}}$;
- average of angular displacement standard deviation values of the camera head around the longitudinal axis $\overline{\sigma_\alpha}$;
- average of angular displacement standard deviation values of the camera head around transverse axis $\overline{\sigma_\gamma}$;
- average of maximum angular displacement values of the camera head around the longitudinal axis $\overline{\alpha_{MAX}}$;
- average of maximum angular displacement values of the camera head around the transverse axis $\overline{\gamma_{MAX}}$.

As a result of the conducted research, it was found that the dominant influence on the ability to recognize and identify an image has the angular velocity around the longitudinal axis and around the transverse axis.

The change in average values of the marker detection efficiency index $h_o$ and marker identification index $h_i$ depending on the average effective values, standard deviations, and maximum angular displacements of the teleoperation system's camera head during the research is presented in Fig. 3. To evaluate the results obtained from the conducted tests, four levels of suspension performance were defined: Excellent, Good, Acceptable, and Unacceptable. These levels are determined by the number of detected obstacles, with the assumption that a performance is deemed "Unacceptable" when less than 90 % of the obstacles are detected.

According to the proposed classification (Table 2), the effectiveness level of the suspension system was divided into four groups. The key indicator for this classification is the value of the marker detection efficiency index $\overline{\eta_o}$. In the context of missions related to driving, detecting, and identifying objects, the failure to find any object is deemed unacceptable. As a result of the discussed research, it was possible to develop universal criteria that can be used to evaluate the suspension systems of teleoperated wheeled UGVs.

## 3. Simulation Studies

The impact of the suspension structure used in the wheeled UGV on the effectiveness of object observation using cameras during off-road driving was studied via simulation. Conducting such experimental studies would be highly challenging in practice and would require substantial financial resources. Therefore, an advanced simulation model of the UGV was constructed, incorporating different suspension structures. During these simulation studies, the platform models moved along a test track (Fig. 4), which imposed a kinematic excitation $q(t)$ with constant specified driving speeds of 4, 5, and 7 km/h (in accordance with ISO 5008 standard).

During recording, selected kinematic features were recorded:
- angular displacement $\alpha(t)$, $\beta(t)$, and $\gamma(t)$,
- angular velocity $\dot{\alpha}(t)$, $\dot{\beta}(t)$, and $\dot{\gamma}(t)$,
- at the center mass position of the platform (Fig. 5).

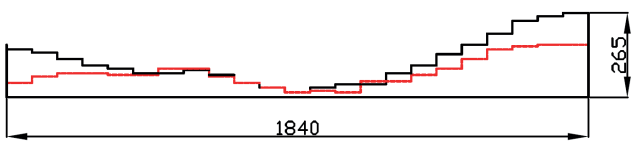


**Fig. 4. Excerpt of the test track used in simulation studies [32]**
Rys. 4. Fragment toru testowego użytego w badaniach symulacyjnych[32]

### 3.1. Unmanned Ground Vehicle model

For the purpose of simulation studies, a numerical model of a 6 × 6 UGV (unmanned six-wheeled ground vehicle) was used, weighing 2800 kg, with an axle base of 1.80 m, wheel track of 1.80 m, and wheel diameter of 0.50 m (Fig. 5). The model was developed using the multi-body method in the Adams 2014.0.1

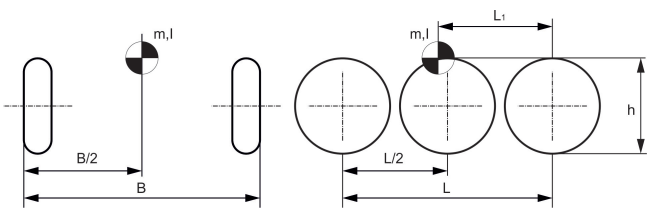


**Fig. 5. Main dimensions of the UGV model [32]**
Rys. 5. Główne wymiary modelu UGV [32]

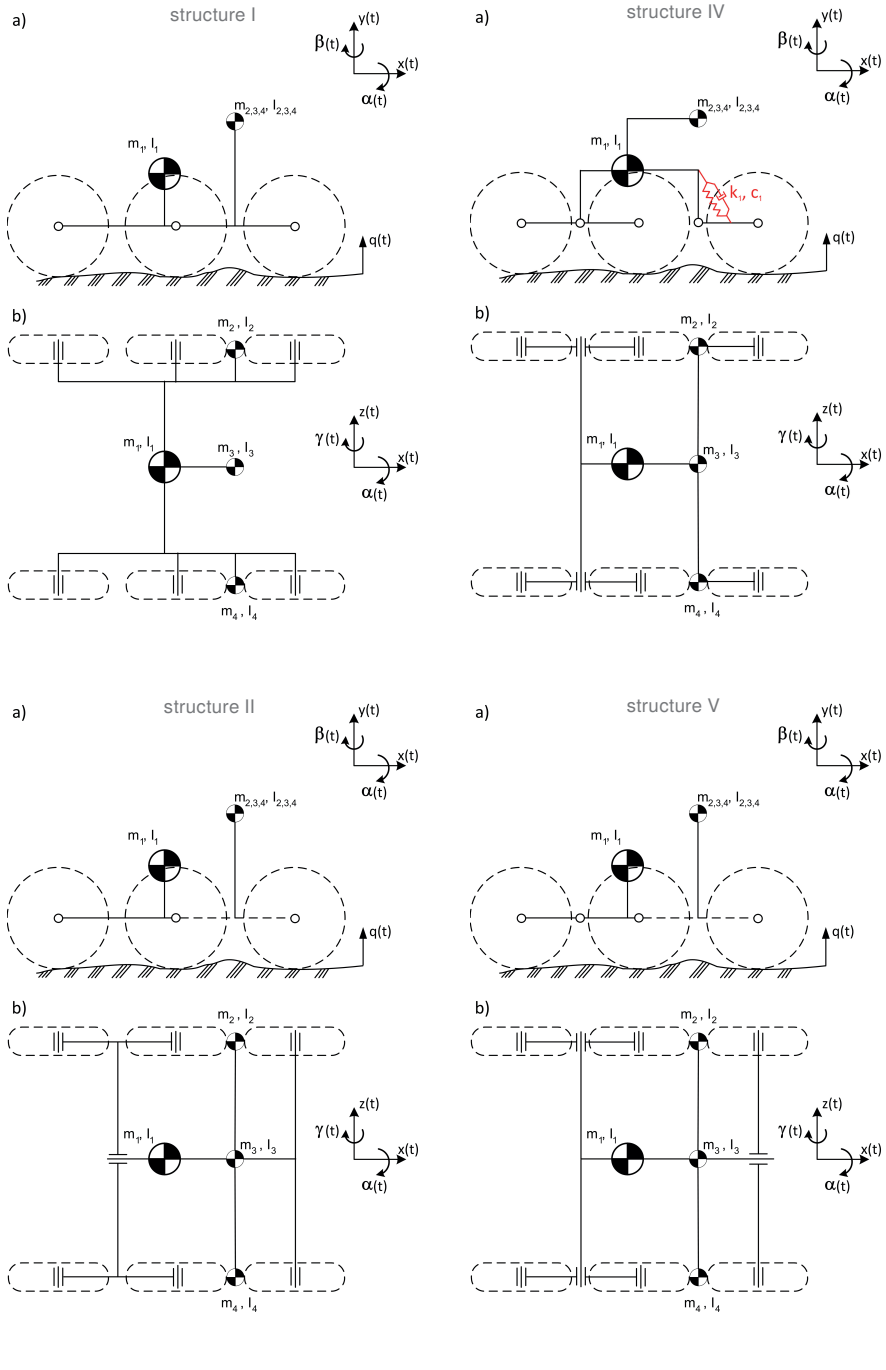


**Fig. 6. Model of UGV Suspension Structures I-V with the orientation of the global coordinate system: a) side view; b) front view; q(t) – kinematic excitation [32]**
Rys. 6. Model struktur zawieszenia UGV I-V w widoku: a) bocznym; b) przednim; q(t) – wymuszenie kinematyczne [32]

software (MSC Software Corporation) [25]. To this end, a set of simplifying assumptions were adopted, including:

- rigid bodies/non-deformable, with homogeneous density throughout their volume,
- reduction of mass and mass moments of inertia to the resultant values m, and I,
- contact forces of wheels with the ground were calculated analytically using the impact force model according to the equation (5),
- ideal kinematic constraints (without friction),
- a constant angular velocity of the driving wheels was assumed during the entire pass on the test track.

The values of masses and mass moments of inertia are presented in Table 3, while the main dimensions and the positions of the centers of gravity are given in Table 4.

## 3.2. Suspension structure in the vehicle model

In the simulation studies, three vehicle structure variants were developed:

- wheels mounted directly to the vehicle frame (Fig. 6a),
- rear axles are attached to longitudinal control arms and the front wheels on a transverse control arm (Fig. 6b, c),
- independent wheel suspension with a shock-absorbing spring (Fig. 6d, e) [16].

**Tab. 3. Masses and moments of inertia of the UGV body and wheel model [32]**
Tab. 3. Masy i momenty bezwładności bryły nadwozia modelu UGV oraz kół jezdnych [32]

| | Name | $m$ [kg] | $I_{xx}$ [kgm²] | $I_{yy}$ [kgm²] | $I_{zz}$ [kgm²] |
|---|---|---|---|---|---|
| 1. | vehicle weight $m$ | 2800 | 25 400 | 25 400 | 25 400 |
| 2. | tire weight $m_{ki}$ | 20.88 | 1.9293 | 0.9778 | 0.9778 |
| 3. | wheel rim $m_{oi}$ | 15.25 | 0.4687 | 0.2625 | 0.2625 |

**Tab. 4. Principal dimensions of the model in numerical analyses [32]**
Tab. 4. Główne wymiary modelu w analizach numerycznych [32]

| | Name | Length [mm] |
|---|---|---|
| 1. | Overall width B | 2010 |
| 2. | Wheelbase distance L1 | 990 |
| 3. | Axle track L | 1800 |
| 4. | Vertical position of the chassis center of mass h | 750 |

### 3.3. Discrete Model of the flexible wheel

In the vehicle model, a discrete wheel model was implemented. It consists of rigid bodies arranged circumferentially in a ring, representing the tire tread. These discrete elements were coupled to the rim using linear forces and moments. Unit stiffness and damping values were chosen based on literature data to achieve the desired resultant stiffness and damping parameters in the circumferential, radial, and lateral directions.

The wheel-ground contact is of a multi-point nature and is influenced by both the wheel deflection and the ground curvature. The forces arising from this contact are computed independently for each $i$-th tread element that is in contact with the ground. The total normal force from the wheel to the ground is derived from the summation of the normal forces of the $n$-number of tread elements.

$$F_N = \sum_{i=1}^{n} F_{Ni} \tag{3}$$

The force occurrence of the $i$-th tread element is determined by the condition:

$$F_{Ni} = \begin{cases} \text{inactive} & \text{if} \quad q_i > q_o \\ \text{active} & \text{if} \quad q_i \le q_o \end{cases}, \quad q_o = 0 \tag{4}$$

where: $q_i$ – the distance between the $i$-th tread element and the ground.

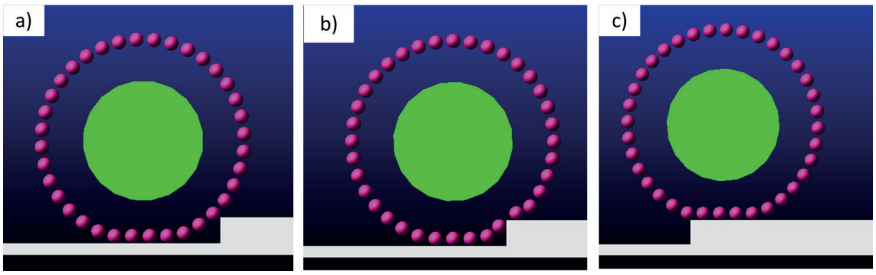


**Fig. 9. View of the wheel model while overcoming a 90 mm height obstacle at a speed of approximately 1 km/h: a), b), c) sequential stages [32]**
Rys. 9. Widok modelu koła podczas pokonywania przeszkody o wysokości 90 mm przy prędkości wynoszącej około 1 km/h: a), b), c) kolejne etapy [32]

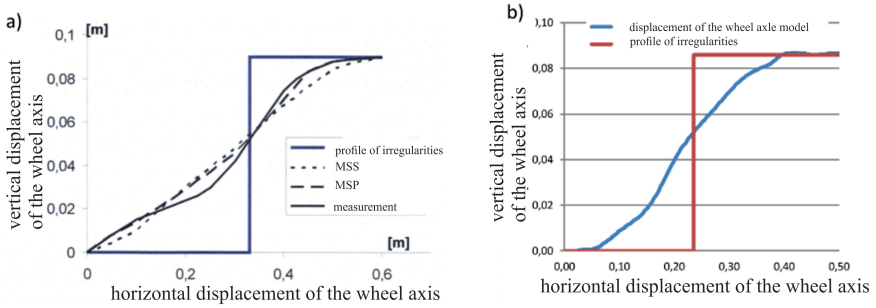


**Fig. 10. Comparison of the wheel center position while overcoming a step-type obstacle: a) comparison of the MSS wheel models (constant tread length model), MSP (model in the form of radially arranged spring-damper links), measurement – result of the measurement conducted on the physical object, b) result of the test conducted on the model (Fig. 9) used in this study [32]**
Rys. 10. Porównanie położenia środka koła podczas pokonywania przeszkody typu występ: a) porównanie modeli koła MSS (model o stałej długości śladu), MSP (model w postaci promieniowo rozmieszczonych łączników sprężysto-tłumiących) pomiar – wynik pomiaru dokonanego na obiekcie fizycznym, b) wynik próby przeprowadzonej na modelu (rys. 9) wykorzystanym w pracy [32]

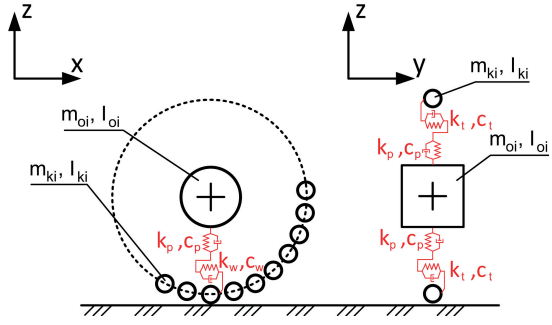


**Fig. 7. Discrete Model of the wheel [32]**
Rys. 7. Dyskretny model koła [32]

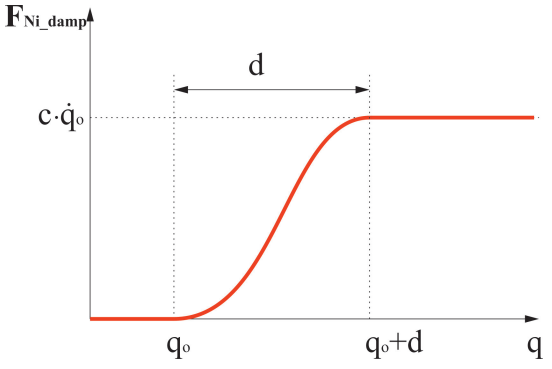


**Fig. 8. Function describing the damping force in the wheel-ground contact [32]**
Rys. 8. Przebieg funkcji opisującej siłę tłumienia w kontakcie koło-ziemia [32]

$$F_{Ni\_stiff} = k_{ground} \cdot \left(q_o - q_i\right)^e \tag{5}$$

where: $k_{ground}$ – ground stiffness, $(q_o - q_i)$ – tread element penetration into the ground, $e$ – exponent determining the shape of the characteristic (according to MSC Adams recommendations, $e = 1.5$) [9].

The damping force depends on the speed, and its rise time depends on the tread penetration into the ground surface. The function describing the increase in damping along with the value of penetration takes a shape similar to the hyperbolic tangent in the range $F_{Ni\_damp} = (0–c_{ground})$ and has been determined based on the equation (Fig. 8):

$$F_{Ni\_damp} = c_{ground} \cdot \dot{q}_o \text{Step}\left(q, q_o 0, \left(q_o + d\right), 1\right) \tag{6}$$

where: $c_{ground}$ – ground damping coefficient; Step(...) – a function describing the gradual increase in value from 0 to 1 as a function of penetration $q_i$.

The wheel's tire model consists of 36 elements, representing the tire tread in accordance with the recommendations provided in [16]. An essential feature of a wheel model is its "absorbing" properties. These influence the trajectory of the wheel's center. In the study, a result of measurement and simulation of the wheel center's positional change while overcoming a bump of 90 mm in height at a speed of approximately 1 km/h was presented. A similar simulation test was performed for the wheel model used in this study.

As a result of the test, a graph depicting the change in the position of the wheel model's center while overcoming an obstacle-type protrusion was plotted (Fig. 10b).

The displacement graph of the wheel axis model presented in Fig. 10b is closely aligned with the measurement (Fig. 10a). Therefore, it was concluded that the adopted wheel model possesses "absorbing" characteristics.

Based on the simulations, an analysis was conducted to evaluate the test results. The following performance indicators were used for evaluation:

- Root Mean Square (*RMS*) value of angular displacements around the longitudinal axis $\alpha_{RMS}$ and the transverse axis $\gamma_{RMS}$;
- Standard deviation value $\sigma$ of angular displacements around the longitudinal axis $\sigma_{\alpha(t)}$ and the transverse axis $\sigma_{\gamma(t)}$;
- Maximum value of angular displacements around the longitudinal axis $\alpha_{MAX}$ and the transverse axis $\gamma_{MAX}$;
- Root Mean Square (RMS) value of angular velocities around the longitudinal axis $\dot{\alpha}_{RMS}$, vertical axis $\dot{\beta}_{RMS}$, and the transverse axis $\dot{\gamma}_{RMS}$;
- Standard deviation value $\sigma$ of angular velocities around the longitudinal axis $\sigma_{\dot{\alpha}(t)}$, vertical $\sigma_{\dot{\beta}(t)}$, and the transverse axis $\sigma_{\dot{\gamma}(t)}$;
- Maximum value of angular velocity around the longitudinal axis $\dot{\alpha}_{MAX}$, vertical axis $\dot{\beta}_{MAX}$, and the transverse axis $\dot{\gamma}_{MAX}$.

## 4. Results

Examples of simulation results obtained during the simulation tests are presented in Fig. 11. They present the time histories of angular velocities and angular displacements recorded at the location of the center of gravity for two variants of road wheel suspension.

Figure 12 shows a graphical comparison of the values of evaluation indicators calculated based on changes in angular displacements around the longitudinal axis $\alpha(t)$ and transverse axis $\gamma(t)$ during simulations.

The analysis of the obtained results indicates that the change in driving speed has a significant impact on the angular displacements of the models around the longitudinal axis (Fig. 12a). Larger differences between angular displacements occurred in the case of displacements around the transverse axis (Fig. 12b). Structure III is the least sensitive to changes in driving speed and, as a result, in angular displacements around the transverse axis. In this case, an increase in driving speed 4–7 km/h resulted

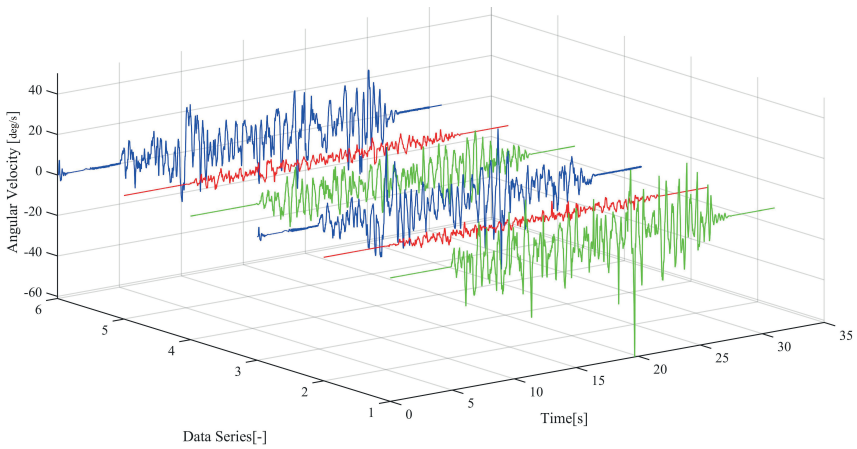


**Fig. 11. Angular velocities time series fragments at a speed of 7 km/h for structure II relative to the axes: 1 – longitudinal, 2 – vertical, 3 – transverse, and for structure III: 4 – transverse velocity, 5 – vertical, 6 – velocity relative to the transverse axis [32]**

Rys. 11. Fragmenty przebiegów czasowych prędkości kątowych nadwozia przy prędkości jazdy 7 km/h i struktury zawieszenia II, względem osi: 1 – podłużnej, 2 – pionowej, 3 – poprzecznej, oraz dla struktury III: 4 – prędkość poprzeczna, 5 – pionowa, 6 – prędkość względem osi poprzecznej [32]

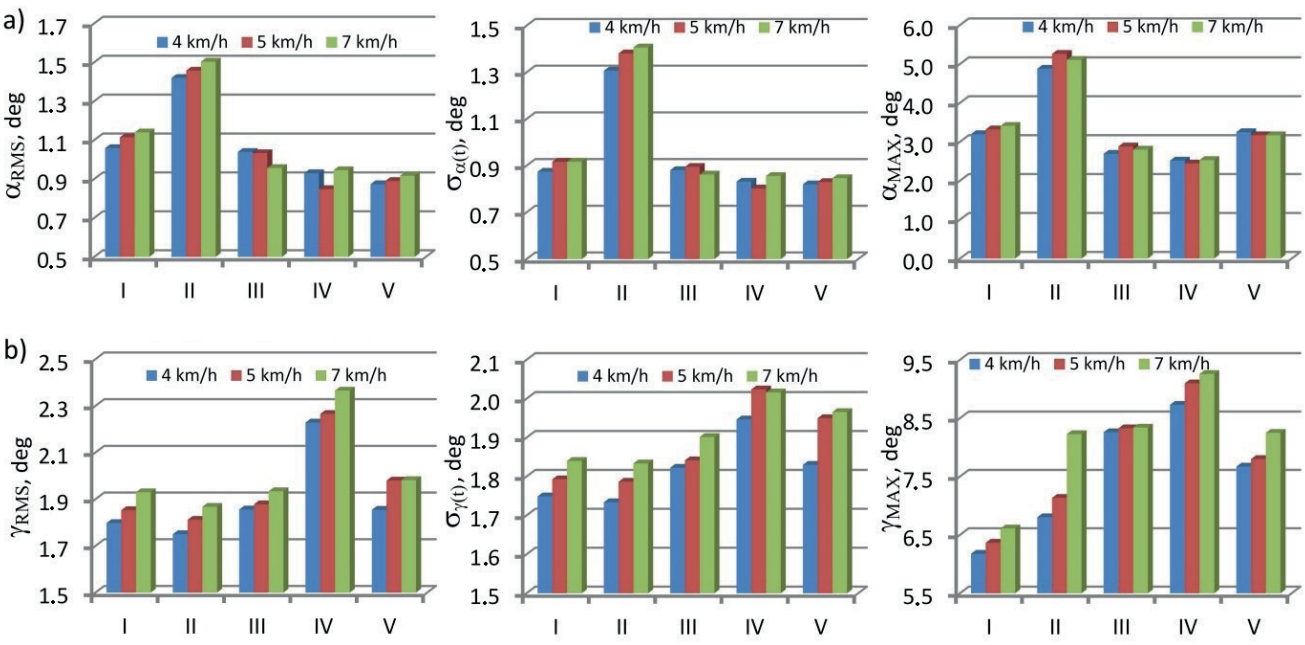


**Fig. 12. Comparison of the values of evaluation indicators (effective values, standard deviation, maximum values) of angular displacements: a) around the longitudinal axis; b) around the transverse axis, I–V – suspensions structure [32]**

Rys. 12. Porównanie wartości wskaźników oceny (wartości skutecznych, odchylenia standardowego, wartości maksymalnych) przemieszczeń kątowych: a) wokół osi wzdłużnej; b) wokół osi poprzecznej, I–V – struktura zawieszenia [32]

in a slight change in the effective value of angular displacements $\gamma_{RMS}$ from 1.86 to 1.93 deg, and the value of standard deviation $\sigma_{\gamma(t)}$ 1.82–1.9 deg and a change in the maximum value of $\gamma_{MAX}$ 8.33–8.34 deg. At the same time, in the case of structure II, a similar change in speed resulted in an increase in the effective value of angular displacement around the transverse axis by 0.15 deg, the value of the standard deviation by 0.12 deg, and the value of the maximum angular displacement by 2.05 deg.

A graphical comparison of RMS values, standard deviations, and maximum angular speeds around the longitudinal, vertical, and transverse axes is shown in Fig. 13.

The largest change in the effective value of angular velocity around the longitudinal axis occurred in the case of structure II (an increase of 4.2 deg/s), constituting approximately 75 % of the velocity value achieved at a driving speed of 4 km/h. The smallest change occurred in structure I (an increase of 1.2 deg/s), which is approximately 35 % of the initial value. The dispersion of the velocity values around the longitudinal axis around the mean value was also the largest in the case of structure II (change by 4.6 deg/s), while the smallest in structure V (1.75 deg/s). The maximum values of angular velocity around the longitudinal axis have changed similarly. In the case of structure II, the increase in the maximum value (Fig. 13a) was close to 20 deg/s (representing approximately 45 % of the maximum value that occurred in the case of driving at a speed of 4 km/h), while in structure V there was an increase in the maximum value of the angular velocity around the longitudinal axis by 5.2 deg/s (thus constituting approximately 45 % of the initial value). The greatest intensity of changes in angular velocity around the vertical axis (Fig. 13b) based on changes in the *RMS* value and standard deviation occurred in the case of structures III, IV, and V (changes of approximately 0.8 deg/s). The smallest in the case of structure I (*RMS* change by 0.2 deg/s). In turn, in the case of examining this structure, the greatest change in the value of the maximum angular velocity around the vertical axis occurred (an increase of approximately 4.8 deg/s). The smallest impact on changes in angular velocities around the transverse axis (Fig. 13c), caused by changes in driving speed, occurred in the case of structure I. The largest change in angular velocities around the transverse axis occurred in structures IV and V.

Figure 14 shows a graphical comparison of the effective values, standard deviation, and values of maximum angular displacements of the tested structures around the longitudinal and transverse axes.

In structure II (Fig. 14a), there was the highest effective value of angular displacements around the longitudinal axis (1.46 deg), the standard deviation value (1.38 deg), and the maximum value (5.26 deg). They were higher than the lowest value in structure IV by 71 %, 73 %, and in the case of the maximum value by 115 %, respectively. Angular displacements around the transverse axis (Fig. 14 b) were the smallest in structures I and II. In their case, there was also the smallest dispersion of displacement values around the average value. By far the highest effective value of angular displacements around the transverse axis occurred in structure IV (2.27 deg) and was greater than the smallest one by approximately 26 %. The highest standard deviation value was also recorded in this structure. The maximum angular displacement around the transverse axis occurred

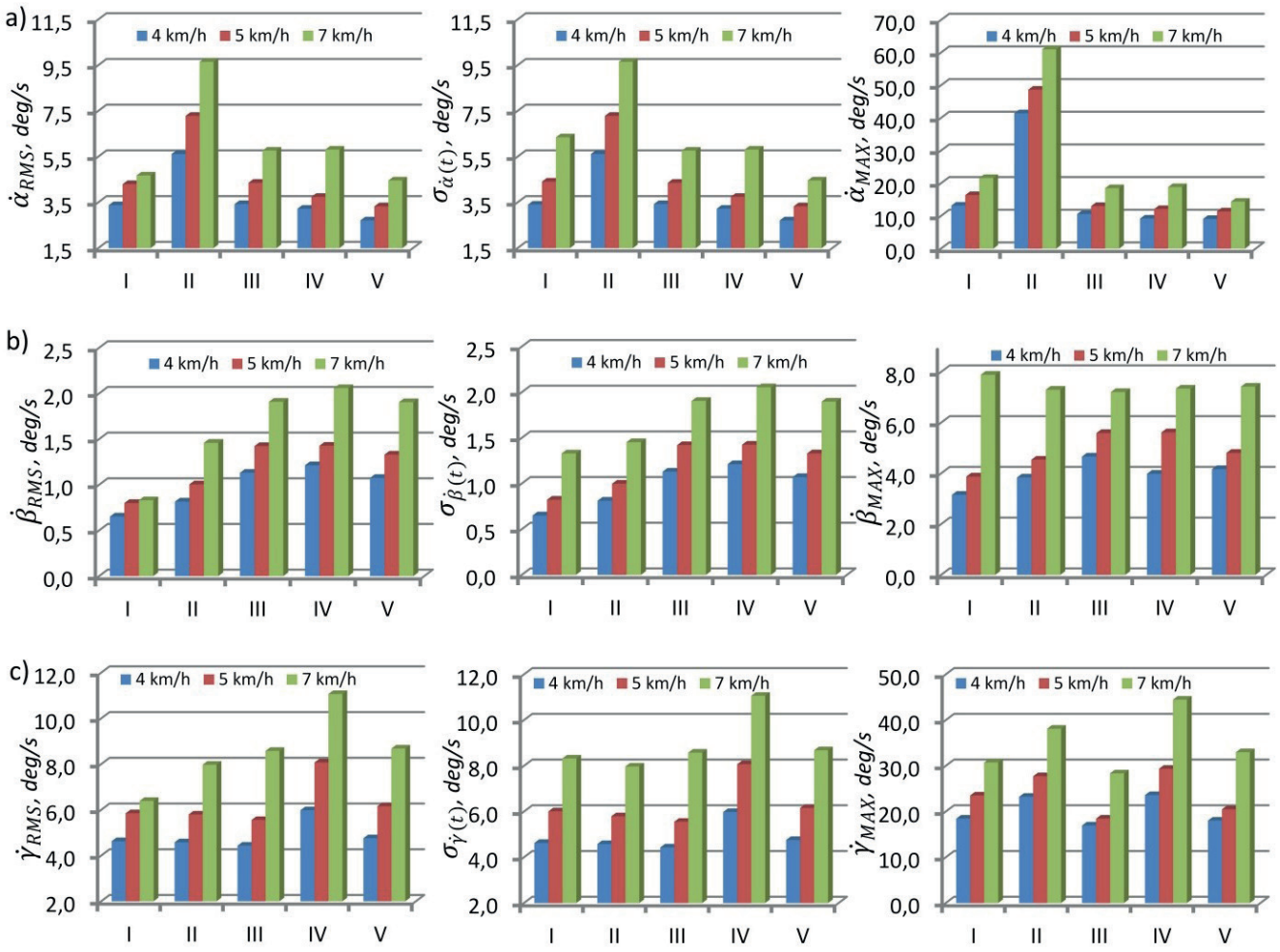


**Fig. 13. Comparison of the values of evaluation indicators (RMS values, standard deviation, maximum values) of angular velocity: a) around the longitudinal axis; b) around the vertical axis; c) around the transverse axis, I–V – suspensions structure [32]**

Rys. 13. Porównanie wartości wskaźników oceny (wartości skutecznych, odchylenia standardowego, wartości maksymalnych) prędkości kątowej: a) wokół osi wzdłużnej; b) wokół osi pionowej; c) wokół osi poprzecznej, I–V – struktura zawieszenia [32]

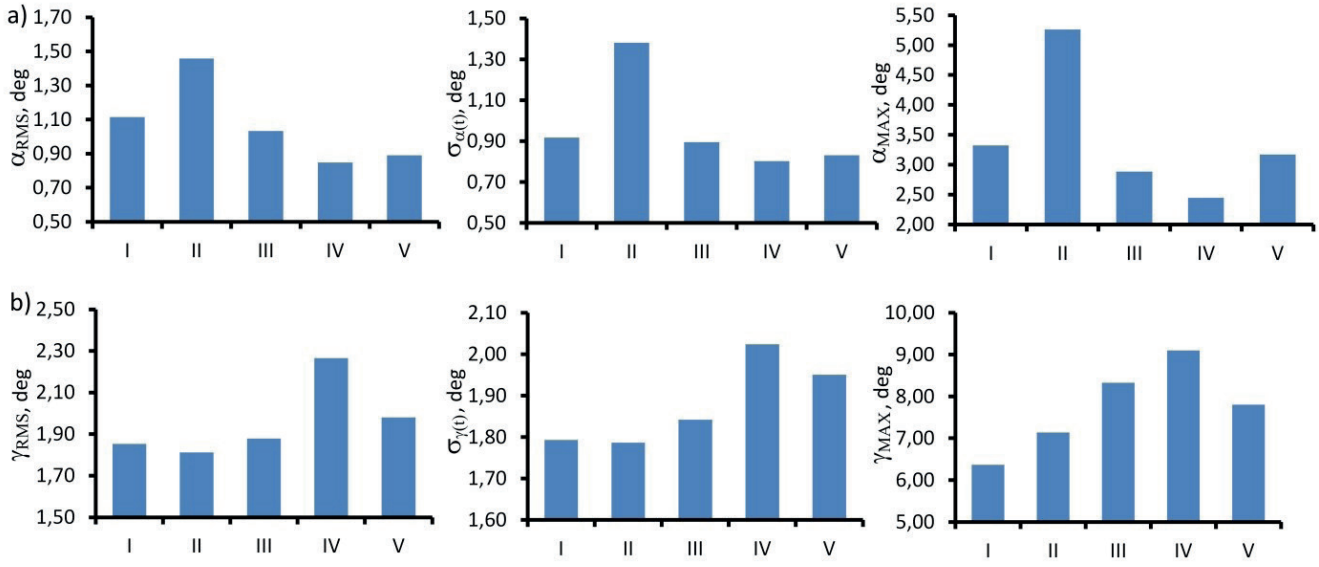


**Fig. 14. Comparison of RMS values, standard deviations, and maximum angular displacements: a) around the longitudinal axis; b) around the transverse axis of the central camera while passing structure models at a speed of 5 km/h, I–V – suspensions structure [32]**
Rys. 14. Porównanie wartości skutecznych, odchyleń standardowych i maksymalnych przemieszczeń kątowych: a) wokół osi wzdłużnej; b) wokół osi poprzecznej, kamery środkowej podczas przejazdu modeli struktur z prędkością 5 km/h, I–V – struktura zawieszenia [32]

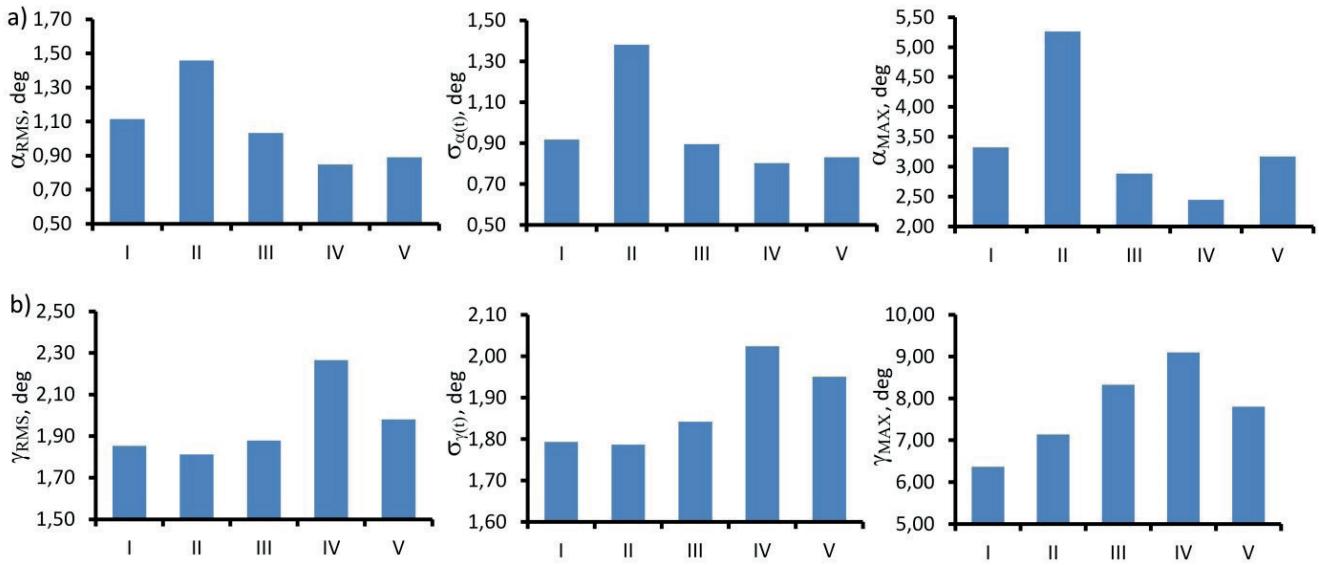


**Fig. 15. Comparison of RMS values, standard deviations, and maximum angular velocities: (a) around the longitudinal axis; b) around the vertical axis; c) around the transverse axis of the central camera while passing structure models at a speed of 5 km/h, I–V – suspensions structure [32]**
Rys. 15. Porównanie wartości skutecznych, odchyleń standardowych i maksymalnych prędkości kątowej: a) wokół osi wzdłużnej; b) wokół osi pionowej; c) wokół osi poprzecznej, kamery środkowej podczas przejazdu modeli struktur z prędkością 5 km/h, I–V – struktura zawieszenia [32]

in structure IV and amounted to 9.1 deg. This result is approximately 43 % greater than the maximum displacement that occurred in structure I.

Figure 15 shows a graphical comparison of RMS values, standard deviations, and maximum angular velocities around the longitudinal, vertical, and transverse axes.

In structure II, there were not only the highest values of angular displacements around the longitudinal axis (Fig. 15a) but also the highest values of velocities around the longitudinal axis. In this case, the effective value of speed and standard deviation was approximately 7.3 deg/s, and the maximum was 48.68 deg/s. These values significantly exceeded the lowest values that occurred in structure V. They were higher than them by 3.96 deg/s and 37.26 deg/s, respectively. In the case of angular velocity around the vertical axis (Fig. 15b), the highest effective and maximum values were achieved by structures III, IV, and V. They were much smaller in structures I and II. The absolute differences between the extreme values were for the effective value and standard deviation approximately 0.6 deg/s, and for the maximum value approximately 1.7 deg/s. The highest values of angular velocity around the transverse axis (Fig. 15c) occurred in structure IV, while the lowest in structure III.

In order to select the best structure, a system for evaluating the obtained results was proposed in which, for each assessed indicator (e.g., *RMS* value of angular displacement), the structures are ranked from the smallest value of a given quantity to the largest value. Then each structure receives pi points from 0 points. (in the case of the highest value of the assessed quantity) up to 1 point. (in the case of the smallest value of the assessed quantity – the best solution). The remaining structures receive intermediate values proportionally. The final value, which is the final assessment of a given structure A (after taking into account all assessment indicators), is calculated based on the relationship:

$$A = a \cdot \sum_{i=1}^{n} \left( k_i \cdot p_i \right) \tag{7}$$

where: $a$ – a parameter that takes the value 1/3 if any of the wheels lost contact with the ground while running on the track or 1 if none of the wheels lost contact with the ground while driving; $k_i$ – weight and – of this assessed quantity; $p_i$ – the value of points awarded to a given structure after assessing $i$ – this value.

Based on the posted research, it was concluded that the angular velocities of the cameras have the greatest impact on the operators' ability to observe the surroundings. Therefore, it was decided that the indicators associated with them had the highest $k_i$ weight value. The AHP (Analytic Hierarchy Process) method was used to determine the value of weights assigned to a given quantity. It is used for the multi-criteria analysis of decision-making problems [23]. Before starting the analysis using it, a definition of the decision-maker's preferences is established and determined using relative importance ratings (Table 4).

In the proposed evaluation system, it was found that the angular velocities of the cameras are the strongly preferred quantity. The values of the weights adopted in the proposed evaluation system for individual indicators are summarized in Table 5.

**Tab. 4. The scale of weights assigned, depending on the importance of individual criteria in the AHP method [32]**
Tab. 4. Skala wag przypisywanych w zależności od ważności poszczególnych kryteriów w metodzie AHP [32]

| Value | Rating of element A against B |
|---|---|
| 9 | And is extremely preferred |
| 7 | A is very strongly preferred |
| 5 | A is strongly preferred |
| 3 | A is poorly preferred |
| 1 | A is equivalent to B |

The structure that obtained the highest number of points in the adopted evaluation system is the best structure. During the tests, the wheels of structures I and II lost contact with the ground several times. In the case of structures III, IV, and V, the wheels did not detach from the ground. The assessment was conducted for driving speeds of 5 and 7 km/h. The final results of the assessment of all indicators considered (Table 5) using the adopted system are graphically presented in Fig. 16.

As a result of the research and evaluation, the best (among) the examined structures for UGV are structures III (swinging) and V (flexible). Ultimately, these structures received a score of 36 points (III – driving speed of 5 km/h) and 33.9 points (V – driving speed of 7 km/h). Structures I and II are by far the worst in both cases. They obtained scores of 7 and 9 points. It should be noted that increasing the driving speed to 7 km/h resulted in the fully flexible structure receiving the best rating.

## 5. Discussion / Conclusions

Selecting the most advantageous structure of the suspension system for performing the task of off-road driving and observing the surroundings, required the development of a method for assessing suspension systems and conducting numerical tests. For this purpose, numerical models of five alternative suspension system structures for UGV were developed, and their tests were conducted while driving on a rectilinear off-road track (ISO 5008) constituting kinematic excitation. In addition, the influence of camera placement and movement speed on the interactions occurring on the cameras was examined.

The most advantageous solution is when the robot is suspended with an independent connection of the wheels to the body frame. The values of the angular velocities of the cameras, which are a critical factor determining the effectiveness of this type of task, have the lowest values and approach the limit values of the range of good effectiveness of the UGV suspension.

**Tab. 5. Summary of the values of weights and indicators to which they refer, adopted in the UGV suspension structure assessment method [32]**
Tab. 5. Zestawienie wartości wag i wskaźników, do których się odnoszą, przyjętych w systemie oceny struktury zawieszeń UGV [32]

| $k_i$ | Rating Index |
|---|---|
| 1 | $\alpha_{RMS}$, $\sigma_{\alpha(t)}$, $\alpha_{MAX}$, $\gamma_{RMS}$, $\sigma_{\gamma(t)}$, $\gamma_{MAX}$ |
| 5 | $\dot{\alpha}_{RMS}$, $\sigma_{\dot{\alpha}(t)}$, $\dot{\alpha}_{MAX}$, $\dot{\beta}_{RMS}$, $\sigma_{\dot{\beta}(t)}$, $\dot{\beta}_{MAX}$, $\dot{\gamma}_{RMS}$, $\sigma_{\dot{\gamma}(t)}$, $\dot{\gamma}_{MAX}$. |

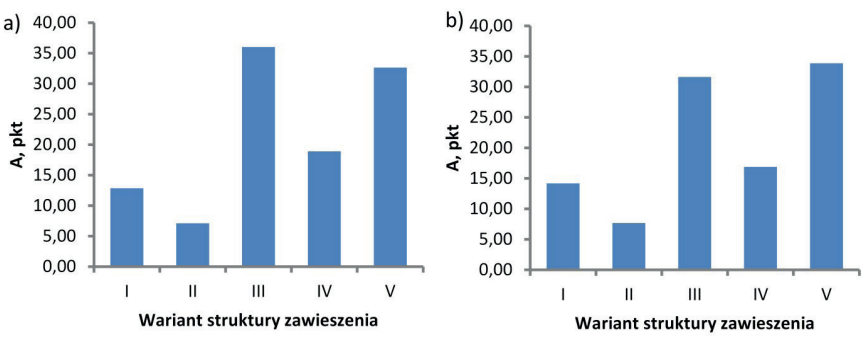


**Fig. 16. Summary of the results of the assessment of suspension system structures using the adopted assessment method: a) at a driving speed of 5 km/h; b) at a driving speed of 7 km/h, I–V – suspensions structure [32]**
Rys. 16. Zestawienie wyników oceny struktur układu zawieszenia z wykorzystaniem przyjętego systemu oceny: a) przy prędkości jazdy 5 km/h; b) przy prędkości jazdy 7 km/h, I–V – struktura zawieszenia [32]

In the next step, a system was created for assessing the suitability of suspension system structures based on a point assessment of several values, such as effective values, standard deviations, and maximum values. Due to the amount of movement of the teleoperation system cameras, the most advantageous solution is to place them in the longitudinal axis of the robot. Depending on the compared parameter, the intensity of the impacts to which the center camera was subjected compared to the side cameras decreased from several to several dozen percent.

Conducting tests at different driving speeds made it possible to assess the structures in terms of their sensitivity to changes in driving speed and its impact on the values that affect the cameras of the teleoperation system. The smallest impact of changes in driving speed on the vibrations of the teleoperation system cameras occurred in the case of structures III and V. Structure I is the most "sensitive" to changes in driving speed. In this case, the calculated evaluation indices at the highest driving speed (7 km/h) were higher than the values calculated at the lowest driving speed (4 km/h) by up to 190 %.

As a result of the assessment, based on the developed system, structure III (the best result for a driving speed of 5 km/h) and structure V (the best result for a driving speed of 7 km/h) were considered the best UGV designs.

Proposed method can be used to evaluate other suspension structures with different velocities and other terrain conditions. This take into account mostly limits of operator perception in objects detection and identification. Future research can focus on adjustment of the UGV suspension characteristics which could have significant influence on situational awareness and the operator's ability to act effectively, especially during dynamic missions.

## Bibliography


1. Almayyahi A., Wang W., Hussein A.A., Birch P., *Motion control design for unmanned ground vehicle in dynamic environment using intelligent controller*, "International Journal of Intelligent Computing and Cybernetics", Vol. 10, No. 4, 2017, 530–548, DOI: 10.1108/IJICC-11-2016-0044.
2. Althani T., Salim R., Anzil M.M., Subramaniam P., Almaeeni K., Shukla A., *Design and Implementation of a Locomotion Suspension System for a Desert Terrain UGV*, "2023 9th International Conference on Automation, Robotics and Applications (ICARA)", Abu Dhabi, United Arab Emirates, 2023, 259–262, DOI: 10.1109/ICARA56516.2023.10125898.
3. Bartnicki A., Muszyński T., Rubiec A., *Hydropneumatic Suspension Efficiency in Terms of Teleoperated UGV Research*, "Solid State Phenomena", Vol. 237, 2015, 195–200, DOI: 10.4028/www.scientific.net/SSP.237.195.
4. Berns K., Nezhadfard A., Tosa M., Balta H., De Cubber G., *Unmanned Ground Robots for Rescue Tasks. Search and Rescue Robotics – From Theory to Practice*, "InTech", 2017, DOI: 10.5772/intechopen.69491.
5. Chen G., Jiang Y., Tang Y., Xu X., *Revised adaptive active disturbance rejection sliding mode control strategy for vertical stability of active hydro-pneumatic suspension*, "ISA Transactions", Vol. 132, 2023, 490–507, DOI: 10.1016/j.isatra.2022.06.008.
6. Chen S., Wang D., Zuo A., Chen Z., Li W., Zan J., *Vehicle Ride Comfort Analysis and Optimization Using Design of Experiment*, "Second International Conference on Intelligent Human-Machine Systems and Cybernetics", Nanjing, China, 2010, 14–18, DOI: 10.1109/IHMSC.2010.11.
7. Chen Z., *Path Planning and optimization of Unmanned Ground Vehicles* (*UGVs*) *in the Field*, "3rd International Conference on Unmanned Systems (ICUS)", Harbin, China, 2020, 708–713, DOI: 10.1109/ICUS50048.2020.9274968.
8. Czapla T., Wrona J., *Technology development of military applications of unmanned ground vehicles*, "Vision Based Systems for UAV Applications", Springer: Heidelberg, Germany, 2013, 293–309, DOI: 10.1007/978-3-319-00369-6_19.
9. Dąbrowska A., Jaskółowski M.B., Rubiec A., *Cameras vibrations influence on efficiency of teleoperated Unmanned Ground Vehicle*, "2016 21st International Conference on Methods and Models in Automation and Robotics (MMAR)", Międzyzdroje, Poland, 2016, 772–777, DOI: 10.1109/MMAR.2016.7575234.
10. Dinelli C., Racette J., Escarcega M., Lotero S., Gordon J., Montoya J., Dunaway C., Androulakis V., Khaniani H., Shao S., *Configurations and Applications of Multi-Agent Hybrid Drone/Unmanned Ground Vehicle for Underground Environments: A Review*, "Drones", Vol. 7, No. 2, 2023, DOI: 10.3390/drones7020136.
11. Fabris E.J., Sangalli V.A., Soares L.P., Pinho M.S., *Immersive telepresence on the operation of unmanned vehicles,* "International Journal of Advanced Robotic Systems", Vol. 18, No. 1, 2021, DOI: 10.1177/1729881420978544.
12. Febriyanto R., Setiawardhana S., Tamara M.N., Sena Bayu B. Dewantara, Sigit R., Sanusi M.A., *Design and Realization of UGV Robot with Combined of Geared Wheel and Walked Mechanism for Uncertain Terrain in Volcanic Observation*, "International Electronics Symposium (IES)", Surabaya, Indonesia, 2022, 317–323, DOI: 10.1109/IES55876.2022.9888626.
13. Gadekar A., Fulsundar S., Deshmukh P., Aher J., Kataria K., Patel V., Barve S., *Rakshak, A modular unmanned ground vehicle for surveillance and logistics operations*, "Cognitive Robotics", Vol. 3, 2023, 23–33, DOI: 10.1016/j.cogr.2023.02.001.
14. Ha C., Lee D., *Vision-based teleoperation of unmanned aerial and ground vehicles*, "IEEE International Conference on Robotics and Automation", Karlsruhe, Germany, 2013, 1465–1470, DOI: 10.1109/ICRA.2013.6630764.
15. Hamid A.A., Nazih A., Ashraf M., Abdulbaky A., Khamis A., *UGV locomotion system for rough terrain*, "2016 International Workshop on Recent Advances in Robotics and Sensor Technology for Humanitarian Demining and Counter-IEDs (RST)", Cairo, Egypt, 2016, DOI: 10.1109/RST.2016.7869858.
16. Hapian-Smith J., *An introduction to modern vehicle design*, Butterworth-Heinemann, Oxford, 2002.
17. Ibicek T., Thite A.N., *Quantification of Human Discomfort in a Vehicle Using a Four-Post Rig Excitation*, "Journal of Low Frequency Noise, Vibration and Active Control", Vol. 31, No. 1, 2012, 29–42, DOI: 10.1260/0263-0923.31.1.29.
18. ISO 2631, Mechanical vibration and shock – Evaluation of human exposure to whole-body vibration, 1997.
19. Kim J., Lee J., *A Testbed for Predicting Maneuverability of UGV on Rough Terrain*, "IFAC Proceedings Volumes", Vol. 46, No. 10, 2013, 132–137, DOI: 10.3182/20130626-3-AU-2035.00044.
20. Krogul P., Cieślik K., Łopatka M.J., Przybysz M., Rubiec A., Muszyński T., Rykała Ł., Typiak R., *Experimental Research on the Influence of Size Ratio on the Effector Movement of the Manipulator with a Large Working Area*, "Applied Sciences", Vol. 13, No. 15, 2023, DOI: 10.3390/app13158908.
21. Luettel T., Himmelsbach M., Wuensche H.J., *Autonomous Ground Vehicles—Concepts and a Path to the Future*, "Proceedings of the IEEE 2012", Vol. 100, 2002, 1831–1839, DOI: 10.1109/JPROC.2012.2189803.
22. Lukoševičius V., Makaras R., Rutka A., Keršys R., Dargužis A., Skvireckas R., *Investigation of Vehicle Stability*

*with Consideration of Suspension Performance*, "Applied Sciences", Vol. 11, No. 20, 2021, DOI: 10.3390/app11209778.
23. Man C.K.Y.L.L., Koonjul Y., Nagowah L., *A low cost autonomous unmanned ground vehicle*, "Future Computing and Informatics Journal", Vol. 3, No. 2, 2018, 304–320, DOI: 10.1016/j.fcij.2018.10.001.
24. Mazal J., Stodola P., Podhorec M., *UGV development with supervised autonomy*, "Proceedings of the 16th International Conference on Mechatronics – Mechatronika 2014", Brno, Czech Republic, 359–363, DOI: 10.1109/MECHATRONIKA.2014.7018284.
25. McConville J., *Introduction to Mechanical System Simulation Using Adams*, SDC Publications, 2015.
26. Mlati M.C., Wang Z., *Unmanned ground vehicles: adaptive control system for real-time rollover prevention*, "International Journal of Vehicle Autonomous Systems", Vol. 16, No. 1, 2021, 81–95, DOI: 10.1504/IJVAS.2021.118047.
27. Muktadir M., Yi S., Hamoush S., Garfo S., Dekkata S.C., Li X., Tereda A.A., McKee R., Brown K., Klawah N., *Uncrewed Ground Vehicles* (*UGVs*) *and Nature-Inspired Designed Robot DIGIT and SPOT: A Review*, "American Journal of Engineering and Applied Sciences", Vol. 15, No. 4, 2022, 274–287, DOI: 10.3844/ajeassp.2022.274.287.
28. Nie C., Hauschka G., Spenko M., *Design and experimental characterization of an omnidirectional unmanned ground vehicle for outdoor terrain*, "IEEE International Conference on Robotics and Automation", Saint Paul, USA, 2012, DOI: 10.1109/ICRA.2012.6225155.
29. Parczewski K., Wnęk H., *The influence of the type of suspensions on vehicle stability and steerability*, "Proceedings of 19th International Conference Transport Means.", 2015.
30. Parekh D., Poddar N., Rajpurkar A., Chahal M., Kumar N., Joshi G.P., Cho W., *A Review on Autonomous Vehicles: Progress, Methods and Challenges*, "Electronics", Vol. 11, No. 14, 2022, DOI: 10.3390/electronics11142162.
31. Rajesh R.J., Kavitha P., *Camera gimbal stabilization using conventional PID controller and evolutionary algorithms,* "International Conference on Computer, Communication and Control (IC4)", Indore, India, 2015, DOI: 10.1109/IC4.2015.7375580.
32. Rubiec A., *Kształtowanie właściwości zawieszeń kołowych teleoperowanych Inżynieryjnych Robotów Wsparcia*, PhD thesis, 2017 (In Polish).
33. Rykała Ł., Rubiec A., Przybysz M., Krogul P., Cieślik K., Muszyński T., Rykała M., *Research on the Positioning Performance of GNSS with a Low-Cost Choke Ring Antenna*, "Applied Sciences", Vol. 13, No. 2, 2023, DOI: 10.3390/app13021007.
34. Someshwaran M., Jose D., Jefferson P.P., *Autonomous unmanned ground vehicle for enhancement of defence strategies*, "Inventive Communication and Computational Technologies: Proceedings of ICICCT 2019", Springer Singapore, 873–880, DOI: 10.1007/978-981-15-0146-3_84.
35. Theunissen J., Tota A., Gruber P., Dhaens M., Sorniotti A., *Preview-based techniques for vehicle suspension control: a state-of-the-art review*, "Annual Reviews in Control", Vol. 51, 2021, 206–235, DOI: 10.1016/j.arcontrol.2021.03.010.
36. Typiak A., *Sterowanie mobilnymi maszynami inżynieryjnymi w układzie teleoperacji*. Wojskowa Akademia Techniczna, 2013, 30–50, ISBN 978-83-62954-82-7 (In Polish).
37. Verma M., Lafarga V., Baron M., Collette C., *Active stabilization of unmanned aerial vehicle imaging platform.* "Journal of Vibration and Control", Vol. 26, No. 19-20, 2020, 1791–1803, DOI: 10.1177/1077546320905494.
38. Wang Y., Liu J., *Evaluation methods for the autonomy of unmanned systems*, "Chinese Science Bulletin", Vol. 57, 2012, 3409–3418, DOI: 10.1007/s11434-012-5183-2.
39. Yu B., Wang Z., Wang G., Zhao J., Zhou L., Zhao J., *Investigation of the suspension design and ride comfort of an electric mini off-road vehicle*, "Advances in Mechanical Engineering", Vol. 11, No. 1, 2019, DOI: 10.1177/1687814018823351.
40. Zhang J., Hou J., Hu J., Zhao C., Xu Z., Cheng C., *UGV autonomous driving system design for unstructed environment*, "40th Chinese Control Conference (CCC)", Shanghai, China, 2021, 4157–4162, DOI: 10.23919/CCC52363.2021.9549342.
41. Zhang K., Yang Y., Fu M., Wang M., *Traversability Assessment and Trajectory Planning of Unmanned Ground Vehicles with Suspension Systems on Rough Terrain*, "Sensors", Vol. 19, No. 20, 2019, DOI: 10.3390/s19204372.
42. Zhang L., Ren C., Yuan X., Zhang W., *Ride comfort control of in-wheel motor drive unmanned ground vehicles with energy regeneration*, "Proceedings of the Institution of Mechanical Engineers, Part D: Journal of Automobile Engineering", Vol. 235, No. 4, 2021, 1057–1069, DOI: 10.1177/0954407020933364.

# Badanie wpływu układu zawieszenia bezzałogowej platformy lądowej na ruch kamery układu teleoperacji

Streszczenie: W poniższym artykule przedstawiono wyniki badań wpływu zastosowanego w bezzałogowej platformie lądowej (BPL) układu zawieszenia na wymuszenia kinematyczne kamer w systemie teleoperacji. Jak wynika z opisanych wstępnych badań rozpoznawczych, te wymuszenia istotnie wpływają na zdolność percepcji operatora oraz jego umiejętność rozpoznawania obrazu podczas jazdy. Obecnie w literaturze brakuje publikacji i wytycznych w zakresie projektowania zawieszeń w BPL oraz ich oceny pod kątem poprawy percepcji operatorów w systemie teleoperacji. Przeprowadzone badania dowodzą, że odpowiednie dostosowanie charakterystyki zawieszenia BPL może znacznie poprawić świadomość sytuacyjną i umiejętność działania operatorów. Badania zostały przeprowadzone w sposób symulacyjny w środowisku przeznaczonym do modelowania układów wieloczłonowych, gdzie opracowano różne warianty struktur zawieszenia. Jako wymuszenie zastosowano model toru testowego ISO 5008 standard. Ocenę badanych struktur zawieszenia przeprowadzono za pomocą autorskiej metody, która pozwoliła na parametryczną analizę i wybór najlepszych rozwiązań pod kątem poprawy rozpoznawania obrazu przez operatora BPL.

**Słowa kluczowe:** układ zawieszenia, system teleoperacji, BPL, świadomość sytuacyjna, model wieloczłonowy

## Arkadiusz Rubiec, PhD, Eng.
arkadiusz.rubiec@wat.edu.pl
**ORCID: 0000-0003-1010-4973**

He received his MSc degree and PhD in mechanical engineering from Military University of Technology in Warsaw, in 2008 and 2017. Currently he is an Assistant Professor at Institute of Robots and Machine Design, Faculty of Mechanical Engineering, Military University of Technology. From 2022 he is Head of Center for Mobile Robot and member of WAT Center for Mobile Robots and Drones. His research interests include designing, constructing and testing innovative technological solutions, in particular dynamic and simulations of unmanned ground vehicles, their manipulators and hydraulic drive systems and factors related to mobile robots operators situational and actional awareness.

## Mirosław Przybysz, PhD, Eng.
miroslaw.przybysz@wat.edu.pl
**ORCID: 0000-0003-2479-7571**

He currently serving as an Assistant Professor at the Institute of Robots and Machine Design within the Faculty of Mechanical Engineering at the Military University of Technology, earned his MSc and PhD degrees in mechanical engineering from the same institution in 2009 and 2019 respectively. His scholarly pursuits focus on the development, construction, and evaluation of cutting-edge technological innovations, with a specific emphasis on unmanned land platforms, transmission system, and hydraulic drive systems.

## Marian Janusz Lopatka, DSc, PhD, Eng.
marian.lopatka@wat.edu.pl
**ORCID: 0000-0003-3449-4611**

He received the MSc degree and the PhD degree in mechanical engineering from the Military University of Technology in Warsaw, in 1986 and 1994, respectively. His research interests include dynamic of manipulators and robot undercarriage systems, drive and control systems, especially for robots and combat engineer equipment.

## Łukasz Rykała, PhD, Eng.
lukasz.rykala@wat.edu.pl
**ORCID: 0000-0002-2301-3280**

He received his MSc degree in automatic control and PhD in mechanical engineering from Military University of Technology (2022). Currently he is an Assistant Professor at Institute of Robots and Machine Design, Faculty of Mechanical Engineering, Military University of Technology. His research interests include Ultra-Wideband positioning, artificial intelligence and unmanned ground vehicles.

## Piotr Krogul, PhD, Eng.
piotr.krogul@wat.edu.pl
**ORCID: 0000-0002-3082-1075**


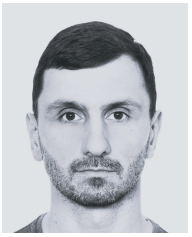

He received his MSc degree and PhD in mechanical engineering from Military University of Technology in Warsaw, in 2009 and 2019. Currently he is an Assistant Professor at Institute of Robots and Machine Design, Faculty of Mechanical Engineering, Military University of Technology. His research interests include designing, constructing and testing innovative technological solutions, in particular unmanned land platforms, their manipulators and hydraulic drive systems.


## Karol Cieślik, PhD, Eng.
karol.cieslik@wat.edu.pl
**ORCID: 0000-0003-4126-2878**


He received his B.Eng. degree in 2012, the MSc degree in 2013 and the PhD degree in mechanical engineering from the Military University of Technology in Warsaw in 2019. Since 2019, he has been working as an Assistant Professor at the Faculty of Mechanical Engineering of the Military University of Technology. He deals with modeling, design, and development of kinematic structures of manipulators and their drive systems. He also conducts simulation and experimental research in terms of changes in hydrostatic parameters of drive systems and their influence on the dynamic properties of manipulators.


## Rafał Typiak, PhD, Eng.
rafal.typiak@wat.edu.pl
**ORCID: 0000-0003-1380-9979**


He received his MSc degree from the Warsaw University of Technology in 2008, and the PhD from the Military University of Technology in Warsaw in 2017. Since then, he has been working as an Assistant Professor at the Faculty of Mechanical Engineering of the Military University of Technology. He deals with developing control systems for robots and other working machines. He also tackles the problems of autonomous operations and swarm management.